Interactions of carbonaceous nanoparticles with a lipid bilayer membrane: A molecular study

Steven L. Fiedler, Angela Violi[*]
Department of Mechanical Engineering
The University of Michigan
Ann Arbor MI 48109-2125

Abstract
Despite established structural and material properties of carboneous nanoparticles, toxicological assessments of only the simplest particles have recently been undertaken. Employing a set of particles systematically ranging in morphology from a representative particle from a combustion environment to the prototypical C_{60} molecule, significant variation was found in the respective permeabilities and free energy potentials. Our analysis is in agreement with the experimentally observed correlation between particle surface area and permeability. The computed results highlight the inadequacy of using the often-employed C_{60} to represent the set of carbonaceous nanoparticles.

Introduction

By number concentration, ultrafine particles of less than 100 nm in diameter constitute the majority of the particulate matter found in the atmosphere [1]. This has raised health concerns since the magnitude of adverse physiological effects due to exposure has been observed to scale inversely with particle size [2]. Nano-sized permeants can enter an organism by ingestion, respiration, and penetration through the skin [2]. By each pathway, particles must penetrate cell membranes comprised of lipid bilayers. The feasibility of this process has been demonstrated by X-ray reflectivity and small-angle neutron scattering (SANS) measurements that have observed cell membrane disruption due to nanoparticle permeation [3]. Computationally, the penetration process has been simulated by molecular dynamics (MD) with concurrent determination of relevant thermodynamic quantities associated with lipid/ nanoparticle interactions [4,5,6,7,8].

To systematically evaluate potential health and the ecological effect of nanoscale materials, an alliance of scientific experts recently announced the formation of the International Alliance for NanoEHS Harmonization, a body designed to standardize toxicological testing protocols [9]. Furthermore, an international regulatory consortium including the United States Environmental Protection Agency has specified a representative set of prototypical manufactured nanoscale materials for toxicological testing [10]. In this set of 14 substances, carboneous particles in the size range of 0.5 - 1.5 nm are represented by only by C_{60} fullerenes and potentially very short single and multiple-walled carbon nanotubes. We note however, that anthropogenic particulate matter found in the atmosphere originate to a large extent from combustion processes. To exemplify, a recent apportionment study from a sampling of various urban centers in the United States, attributed motor vehicles as contributing 20% - 76% to the total particulate matter sized less than 2.5 μm (PM2.5) [11]. The resultant nano-sized organic carbon (NOC) particles thus deviate in morphology from the above oft-studied prototypical fullerenes. This has particular importance since particle toxicity has been attributed to high particle surface area to mass ratio that can enhance chemical reactivity and an altered electronic structure with respect to the material in its bulk form, which can facilitate its role as oxidant [12].

Specific Objectives

This study explored the variability of associated diffusion values of a set of NOC particles passively permeating a lipid bilayer. In this context, we present calculated free energy profiles and permeability coefficients of three nano-particles translocating a representative lipid bilayer, dimyristoylphosphatidyl-choline (DMPC)/cholesterol, to: A) elucidate the effects of particle morphology on the permeation process, and B) establish means for the prediction of permeation properties of similarly sized NOC particles. To this end, we employed Molecular Dynamics (MD) to determine the influence of specific permeant size based parameters that can regulate permeation including a comparison of particle mass, surface area, and volume.

Results and Discussion

Three nanoparticles were included in this study: a closed and an open C_{60} fullerene termed C_{60} and open-C_{60} respectively, and a naturally occurring particle from a representative flame environment termed NanoC.

Coordinates for C_{60} (Fig. 1a) were obtained from the default coordinates from Gaussview 3 [13]. The open-C_{60} molecule (Fig. 1b) was created by artificially paring down a C_{100} fullerene with pentagonal and hexagonal faces [14], to a 60 carbon atom structure. The Atomistic Model Particle Inception (AMPI) program [15] was employed to obtain a representative nanoparticle, $C_{68}H_{29}$, as produced from a combustion source (Fig. 1c). Based on the principle of combining the Kinetic Monte Carlo and MD techniques to bridge timescales between and during reaction events, AMPI has been shown to be a capable and computationally tractable approach to calculate the structure of NOC particles of up to hundreds of atoms [16, 17, 18].

Fig. 1   (a) C_{60}, (b) Open-C_{60}, (c) NanoC: Structure of a NOC particle from a propane flame environment.

For MD simulation, the DL_POLY 2.17 GUI [19] was used to generate nanoparticle intramolecular forces. Improving upon previous studies [7, 20] rigid constraints were not imposed on the bonds and angles, which allowed the particle to possess a more realistic, flexible structure. The DMPC and cholesterol force fields were taken from the United Atom OPLS (UA-OPLS) based parameterization [21,22] of Berkowitz and co-workers, and permeant nonbonded potential parameters were similarly assigned UA-OPLS values for consistency. Water molecules were specified by the TIP3P parameterization [22], and all lipid and water bonds were constrained with the SHAKE algorithm. The equations of motion were integrated using GROMACS simulation package version 3.3.1 in single precision [23].

The initial bilayer system configuration consisted of a 3.26 x 4.37 x 7.27 nm3 box containing 48 DMPC molecules interspersed with 16 cholesterol molecules, and solvated above and below with 1372 H2O molecules. The bilayer norm was defined to be parallel with the z-coordinate axis, with distance z originating from the bilayer center and extending 3.4 nm into the aqueous phase. Periodic boundaries conditions were used in all directions. van der Waals and Coulomb cutoffs were set to 1.5 nm and the particle mesh Ewald summation was used for electrostatic interactions with the default associated parameters. Simulations were performed in the isothermal-isobaric ensemble at a temperature of 308 K and a pressure of 1 atm maintained by a Berendsen

thermostadt [24] (τ = 0.1 ps) and Parrinello-Rahman barostat [25] (τ = 1 ps) respectively. Pressure coupling was applied in a semi-isotropic fashion to decouple expansion in the xy-plane from that along the z-coordinate axis.

To calculate free energy values and diffusivity, the three nanoparticles were inserted in voids grown in 1 Å increments along the bilayer norm resulting in 35 separate positions for each nanoparticle. Calculations of the free energy profiles as a function of position along the bilayer norm were carried out using the constraint force (CF) approach, as implemented in the GROMACS 'pull code' with positions of the particles constrained to the xy-plane. The systems were equilibrated for at least 4 ns during which the average normal forces were observed possess significant fluctuation and subsequently collected data for 16 ns. Mean force uncertainties were calculated by the correlation analysis method [26] and propagated from the water phase toward the bilayer center for the integrated free energy values. The depths of the free energy binding of particles in the bilayer center were also calculated by the thermodynamic integration (TI) method using the GROMACS 'free energy code'. To this end, free energy differences were calculated by application of the relevant thermodynamic cycle and by scaling the particles' nonbonding interactions with the environment. A set of eleven coupling parameter (lambda) values, {0, 0.05, 0.1, 0.2, 0.3, ..., 1.0} were used with a soft core sigma value of 0.3, scaling value of 0.5, and power value of 1.0, for the. particles constrained inside and outside the bilayer at z = 0 nm, and 3.4 nm respectively. The TI calculations were run for 2 ns and we excluded the first 0.5 ns for equilibration

The calculated free energy profiles (Fig. 2) of the three permeants possess a barrier absence with respect to transition from the aqueous to the lipid phase and bear similarities in form to the barrier-less profile of C_{60}, calculated by Bedrov et al. [5]. Extending use of the calculated free energy profile of C_{60} (Fig. 2a) to serve as a point of reference for comparison to previous nanoparticle permeation studies, the free energy minimum offset from the bilayer center, z = 1.1 nm, is comparable with the reported 0.7 and 1.1 nm offset of C_{60} permeating DMPC [5] and DPPC bilayers [6] respectively, with difference to the former attributed to variances in the force field parameterization sets used. The depth of the binding, 84 kJ/mol matches the previous reported value in the DMPC bilayer [5], but is a factor of 2.4 larger than the 35 kJ/mol calculated in the DPPC bilayer system [6]. The latter difference may be due to differences in bilayer composition and a lower simulation temperature used for this study. Finally, as a point of validation, the calculated TI ΔG value of -77 kJ/mol in the bilayer center, matches closely the CF value of -69 ± 6 kJ/mol, with the difference attributed to equilibration.
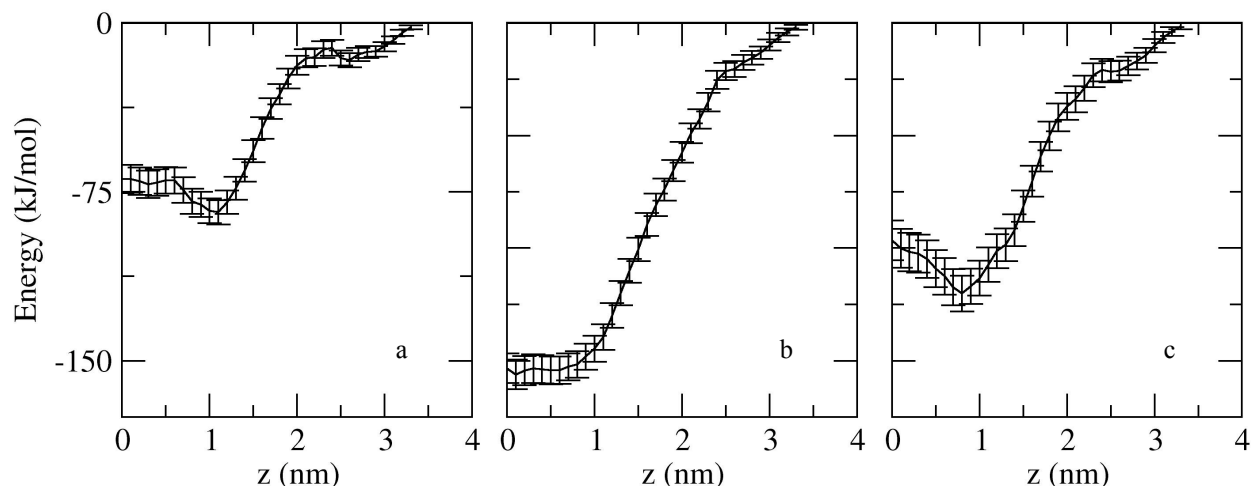
Fig. 2. Particle free energy differences between the water phase and depth z, along the bilayer norm with lines denoting CF values for (a) C_{60}, (b) NanoC, and (c) open-C_{60}.

The free energy profile of the comparably massed NOC particle, NanoC (Fig. 2b), differs from the C_{60} permeant in both profile and depth. Unlike the offset C_{60} free energy minimum, the location of the NanoC minimum is within statistical error of the bilayer center. The free energy profile of NanoC is significantly deeper than C_{60} for all locations within the bilayer and the NanoC binding energy at $z = 0.1$ nm, 156 ± 6 kJ/mol, is to the authors' knowledge, the highest reported of any non-biological permeant in a lipid membrane to date. The calculated TI ΔG value of -151 kJ/mol at the bilayer center falls within the uncertainty of the CF calculation.

The influence of size on the free energy profile of the permeants may be reflected by the number of carbon atoms per molecule, N; i.e., an increased number of non-bonded interactions, or to a aspects related to particle morphology including exposed surface area, molecular volume and molecular atom number density, which could govern the strength of the non-bonded interactions. To explore the influence of particle morphology on the free energy differences between C_{60} and NanoC, we calculated the free energy profile of a protypical, open-C_{60} permeant (Fig. 2c). Since the open-C_{60} possessed an identical N as C_{60}, we attributed differences in free energy to differences in morphology. The open-C_{60} particle size, surface area and volume, exceeded that of C_{60}, but was less than that of NanoC, allowing for its use as a suitable "intermediate". The calculated open-C_{60} free energy values fall between C_{60} and NanoC, for all positions within the bilayer. The free energy minimum is offset from the bilayer center by 0.8 nm, less than that of C_{60}, which may be another indication of the intermediate behavior of the particle. The TI calculation at $z = 0$ nm with a ΔG value -109 kJ/mol, measured closely to the CF value of -96 $\pm$ 9 kJ/mol. The binding depth, 120 kj/mol,

is a factor of 1.4 larger than C_{60} and 0.8 less than NanoC. The calculated permeant atom number densities 101, 92, and 63 atoms/Å^3 for C_{60} and open-C_{60}, and NanoC respectively, demonstrate a loose inverse correlation to the binding energy ratios. Permeant size corresponded more closely to the binding energy ratios, with a surface area ratio of open-C_{60}/C_{60} of 1.2 and open-C_{60}/NanoC ratio of 0.7. Volume ratios compared less favorably at 1.09 and 0.69 respectively.

Local diffusion constants, $D(z)$, were calculated as a function of the autocorrelation function of the instantaneous force [27]. To increase statistical averaging, the 16 ns of instantaneous normal force values acting on the particles' center of mass, were split into 160 bins containing 100 ps each. Force autocorrelation functions were calculated for each bin using multiple time origins and a biased averaging, with a cut-off set at 50 ps. For consistency, the autocorrelation asymptote was defined as zero at 40 ps. The permeation resistance $R(z)$ and subsequently the permeability coefficient, P, were calculated by the inhomogeneous solubility-diffusion approach [27]. Resistance plots (Fig. 3) display similar profiles for the three hydrophobic permeants considered in this study with minimal resistance encountered in the alkane tail region of the bilayer at $z = 1.1$ nm for all molecules. The resistance increases sharply as the permeants' positions approach the aqueous phase and upon exiting the bilayer the resistance profiles possess a much lower slope. The resultant calculated permeability coefficients of C_{60}, open-C_{60}, and NanoC were 383 cm/s, 278 cm/s, and 243 cm/s, attenuating with respect to size. The C_{60} permeability coefficient appears to be a factor of 2.5 greater than that reported by Bedrov et al [5], which may again be due to force-field parameter differences.

3
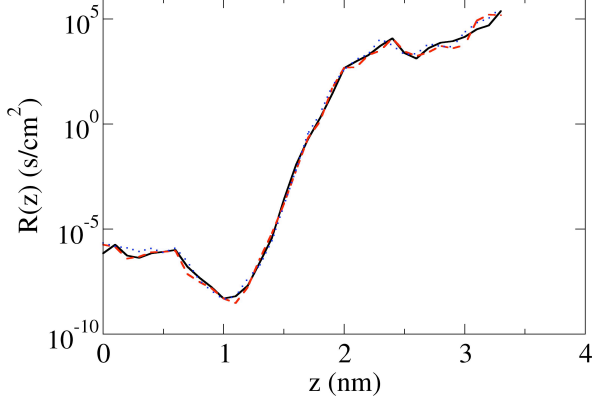
Fig. 3. Particle resistance along the bilayer normal of C_{60} (black line), NanoC (dotted blue line), and open-C_{60} (dashed red line). References to color in this figure are visible in the electronic version of this article.

Fig. 4. Ratio of the permeability and partition coefficient as a function of total surface area (Å^2),

The correlation between a permeant size and permeability is often expressed in the terms of the homogeneous limit of the inhomogeneous solubility diffusion model, the latter defined as,

$$\frac{1}{P} = c_{bulk} \int_0^d \frac{dz}{c(z)D(z)} \qquad (1)$$

for a nonelectrolyte permeability coefficient P, gradient free permeant concentration c, in the bulk and membrane interior, and diffusion coefficient, D [28]. Simplification of Eq. (1) is achievable by stipulating that permeant diffusion is governed by a rate limiting region of length, l [29]. This allows for expression of the permeability as a function of a size dependent parameter A,

$$\frac{P}{K} = \frac{D_O A^{-s}}{l}, \qquad (2)$$

where the diffusion coefficient in the barrier region is represented in Eq. (2) as a quotient of constant D_O and A^s, and the partition coefficient, K, is defined as the concentration ratio. Noting that A has been empirically represented by permeant mass, cross-sectional area and volume [29, 30, 31] we gave consideration in this study to the exposed surface area due to its proportionality to the number of contributing nonbonded interactions. Regression of the logarithmic-logarithmic plots, e.g., Fig. 4, of the P/K ratio as a function of permeant mass, M, surface area, SA, and volume V, allowed determination of the exponential value, s.

The range of Pearson product-moment correlation coefficient values, r, in this study, 0.7-0.9, significantly exceeded the reported value of 0.4 calculated for smaller permeant systems [29], however this may be due to the limited sample size. In this study, the correlation coefficient value based on surface area was 25% higher than with respect to mass. Since the permeability coefficient is a dependent variable of free energy, the higher surface area correlation coefficient value validates with the free energy ratios calculated above. Simply put, for the classification of nanoparticle permeants included in this study, the surface area appears to be the size parameter that possesses the greatest influence on the permeation process.

	s	Intercept	r
Mass	1.8	17.0	0.73
Surface Area	0.73	9.4	0.91
Volume	0.80	10.2	0.84

Table 1. Regression parameters and correlation values of the permeation of carboneaous permeants

Conclusions
The work reported in this paper computationally measures the morphological influence of nanoparticles interacting with cellular systems. We found significant differences in the permeation properties of similarly sized nanoparticles, which may limit the representative capabilities of the C_{60} fullerenes. The correlation established between the permeant surface area and the

depth of the free energy potential, provides a predictive parameter for future studies.

Acknowledgements

References

[1] Y. Zhu, W. C. Hinds, S. Kim, C. Sioutas, J. Air and Waste Manage. Assoc. 52 (2002) 1032-1042.

[2] G. Oberdorster, E. Oberdorster, J. Oberdorster, Environ. Health Perspect. 113 (7) (2005) 823-839.

[3] U. S. Jeng, C. H. Hsu, T. L. Lin, C. M. Wu, H. L. Chen, L. A. Tai, et al. Physica B 357 (2005) 193-198.

[4] J. Wong-Ekkabut, S. Baoukina, W. Triampo, I-M. Tang, D. P. Tieleman, L. Monticelli, 3 (2008) 363-368.

[5] D. Bedrov, G. D. Smith, H. Davande, J. Phys. Chem. B 112 (2008) 2078-2084.

[6] R. Qiao, A. P. Roberts, A. S. Mount, S. J. Klaine, P. C. Ke, Nano Lett. 2007, 7, 614-619.

[7] R. Chang, A. Violi, J. Phys. Chem. B 110 (2006) 5073-5083.

[8] R. A. Tasseff, D. I. Kopelevich, J. Undergrad. Res. 7 (4) (2006).

[9] B. Erickson, Chem. Eng. News 86 (50) (2008) 25-26.

[10] Nanotechnology under the toxic substances control act. URL: http://www.epa.gov/oppt/nano. Accessed 3/9/09.

[11] M. Abu-Allaban, J. A. Gillies, A. W. Gertler, R. Clayton, D. Proffitt, Environ. Monit. 132 (2007)155–163.

[12] A. Nel, T. Xia, L. Mädler, N. Li, Science 311 (2006) 322-627.

[13] GaussView, Version 3.09, Dennington II, R.; Keith, T.; Millam, J.; Eppinnett, K.; Hovell, W. L.; Gilliland, R. Semichem, Inc., Shawnee Mission, KS, 2003.

[14] http://www.cochem2.tutkie.tut.ac.jp/Fuller/higher/higherE.html, accessed Jan. 17, 2008.

[15] A. Violi, Combust. Flame 139 (2004) 279-287.

[16] A. Violi, A. F. Sarofim, G. A. Voth, Combust. Sci. Technol. 176 (2004) 991–1005.

[17] A. Violi, G. A. Voth, A. F. Sarofim, Proc. Combust. Inst. 30 (2005) 1343–51.

[18] A. Violi, A. J. Venkatnathan, J. Chem. Phys. 125 (2006) 054302.

[19] W. Smith, T.R. Forester, J. Mol. Graphics, 14 (1996) 136.

[20] A. Violi, R. W. Chang, Abstract of Papers of the Am. Chem. Soc. 231 (2006) 105.

[21] A. M. Smondyrev, M. L. Berkowitz, Biophys. J. 77 (1999) 2075-2089.

[22] A. M. Mondyrev, M. L. Berkowitz, J. Comp. Chem. 20 (1999) 531-545.

[23] D. van der Spoel, E. Lindahl, B. Hess, G. Grenhof, A. E. Mark, H. J. C. Berendsen, H., J. Comp. Chem. 26 (2005) 1701-1718.

[24] H. J. C. Berendsen, J. P. M. Postma, W. F. van Gunsteren, A. Dinola, J. R. Haak, J. Chem. Phys. 81 (1984) 3684-3690.

[25] M. Parrinello, A. J. Rahman, J. Appl. Phys. 52 (1981) 7182.

[26] W. C. Swope, H.C. Andersen, P. H. Berens, K. R. J. Wilson, J. Chem. Phys. 76 (1982) 637-649.

[27] S.-J. Marrink, H. J. C. Berendsen, J. Phys. Chem. 98 (1994) 4155.

[28] J. M. Diamond, Y. J. Katz, Membrane Biol. 17 (1974) 121-154.

[29] D. Bemporad, C. Luttmann, J. W. Essex, Biophys. J., 87 (2004) 1-13.

[30] S. Lieb, W. D. Stein, Nature, 224 (1969) 240-243.

[31] T. -X. Xiang, B. D. Anderson, J. Membr. Biol. 140 (1994) 111-122.